atmosphere

MDPI

Article

No Response of Surface-Level Atmospheric Electrical Parameters in Israel to Severe Space Weather Events

Roy Yaniv [1,2], Yoav Yair [2,*], Colin Price [3] and Yuval Reuveni [4,5]

[1] Institute of Earth Sciences, The Hebrew University of Jerusalem, Jerusalem 9190501, Israel; roy.yaniv@mail.huji.ac.il
[2] School of Sustainability, Reichman University, Herzliya 4610101, Israel
[3] School of Geosciences, Tel Aviv University, Tel Aviv 6997801, Israel; cprice@flash.tau.ac.il
[4] Department of Physics, Ariel University, Ariel 4070000, Israel; yuvalr@ariel.ac.il
[5] East R&D Center, Ariel 4070000, Israel
* Correspondence: yoav.yair@runi.ac.il; Tel.: +972-99527953 or +972-525415091

Abstract: We report ground-based measurements of the atmospheric electric field (Ez = −potential gradient (PG)) and current density (Jz) that were conducted at two locations in Israel. One is at the Emilio Segre cosmic ray station located on Mt. Hermon (34.45° N, 2020 m AMSL) in northern Israel near the Syrian-Lebanon border, and the other is at the Wise astronomical observatory in the Negev desert highland plateau of southern Israel (31.18° N, 870 m AMSL). We searched for possible effects of strong, short-term solar events on the potential gradient and the vertical current density, as disruptions to the global electric circuit are often observed following strong solar events. The first case study (St. Patrick's Day, 17 March 2015) was classified as the strongest event of 2015. The second case study (8 September 2017) was categorized as the strongest event of 2017 and one of the twenty strongest events on record to date. The results show that the electrical parameters measured at ground level at both stations were not affected during the two massive proton events and the ensuing geomagnetic storms. The magnetospheric shielding in lower latitudes is strong enough to shield against the flux of energetic particles from solar events, obscuring any impact that may be noticeable above the local daily variations induced by local meteorological conditions (aerosol concentrations, clouds, high humidity, and wind speed), which were investigated as well.

Keywords: space weather; global electric circuit; fair weather; electric field; current density; solar proton events; coronal mass ejection

Citation: Yaniv, R.; Yair, Y.; Price, C.; Reuveni, Y. No Response of Surface-Level Atmospheric Electrical Parameters in Israel to Severe Space Weather Events. *Atmosphere* **2023**, *14*, 1649. https://doi.org/10.3390/atmos14111649

Academic Editors: Alla Suvorova and Alexei Dmitriev

Received: 1 October 2023
Revised: 24 October 2023
Accepted: 29 October 2023
Published: 3 November 2023

1. Introduction

Earth's atmosphere undergoes continuous interactions with various types of energetic particles coming from space and from the sun. Solar energetic particles (SEPs) contain 100s of KeV electrons and tens of MeV protons, which deposit their energy in the atmosphere, altering the chemistry and the ionization in the upper atmosphere [1]. Coronal mass ejections (CMEs) and solar flares feature thermal particles moving with a magnetized plasma that are expelled from the sun with velocities of hundreds to thousands of km s^{-1} [1]. Upon arrival at Earth, CMEs and solar flares interact with the magnetosphere [2], thus generating enhanced and disruptive geomagnetic storms. Geomagnetic storms occur when the solar magnetic shock front reconnects with Earth's geomagnetic field, generating ring currents [1,3]. The rapid decrease in the intensity of galactic cosmic ray (GCR) radiation reaching Earth following a solar event is caused by the magnetic field of the solar wind sweeping some of the GCR flux away from Earth in what is known as the Forbush decrease [4,5]. The Forbush decrease can be detected by ground muon detectors for the duration of the impact, which can be several hours long, with a gradual recovery of the cosmic ray flux in the next hours to days [6]. A typical Forbush Decrease has a magnitude of 4–5% of the normal value as measured at ground level by neutron monitors. The Forbush

decrease can have different magnitudes that depend on the position of the CR detector in Earth's geomagnetic field. The rate of occurrence of the phenomena depends on the 11-year cycle of the sun and is more frequent during years of solar maximum. A strong FD (only a few have occurred during solar cycle 24) can produce this magnitude of decrease, even for stations with high cutoff rigidity, as in Israel. The GCR ionization rate exhibits around a 10% difference from solar maximum to solar minimum [4,7].

The global electric circuit (GEC) is a conceptual scheme that refers to the electrical activity in the medium between two conducting plates—the lower ionosphere and the highly conducting Earth—which both serve as the top and bottom plates of a postulated "spherical capacitor". Together with the atmospheric dielectric medium between them and the thunderstorms that act as generators, they define a closed circuit in which a vertical current (Jz) flows to the ground in fair-weather regions [1,3,8]. Short-term variations in the ionization rate at higher altitudes due to changes in the GCR flux, which can last from several hours to several days due to solar events and other SEP events that can produce short-term GLEs (Ground Level Enhancements; [9]), will affect the GEC by altering the conductivity and the columnar atmospheric resistance. Therefore, and in compliance with Ohm's law, we should expect changes in the vertical electric E-field (Ez) or the potential gradient (PG = −Ez).

Ground measurements during times of solar events affecting the Earth at polar latitudes show a decrease in the potential gradient from fair-weather values (~−130 V m^{-1} at sea level) to tenths and even zero V m^{-1} values. The decrease in the potential gradient in polar latitudes is a result of the increased conductivity, an effect of the enhanced ionization due to the injection of charged particles, e.g., electrons, protons, and ions, which are funneled to the polar latitudes by the Earth's magnetic field [1,10–13].

Contrary to the above, ground measurements conducted at high- and mid-latitudes at times of SEPs and CMEs show an increase in the potential gradient and in the conduction current (Jz). This was observed on the day of the impact and in subsequent days [9,14,15]. Mid-latitude measurements of the PG and Jz conducted by the network of middle and high-latitude observatories in Europe (~45–60° N) following six events of Forbush decrease showed an immediate increase when the GCR ionization rate was at a minimum [16]. Measurements of the PG at Swider, Poland (52.2° N geographic, 53.9° N magnetic, geomagnetic rigidity cutoff ~3 GV) during 14 strong and moderate magnetic storms occurring in days defined as fair weather (based on meteorology) found an influence of the solar events on the PG which exceeded local fair-weather variation by ~150 V m^{-1}. The PG amplitude changes were correlated with the times of Forbush decrease events [17]. Qiu et al. (2022) reported 15 cases of increased geomagnetic activity at mid-latitudes, which found variations that range between 100 and 600 V m^{-1} compared to fair-weather values. Ground measurements of the potential gradient in Kamchatka, Russia (57° N geographic, 58.5° N magnetic) showed amplitudes of up to 300 V m^{-1} during a geomagnetic storm in 2010 [18].

Airborne stratospheric measurements during a solar flare at high- (50–70° N) and low- (<50° N) latitudes found a short-duration increase by a factor of 2 in the current density (Jz) at high latitudes but no effect in lower latitude [10,11]. Simultaneous ground and airborne measurements were performed at Reading, UK (51.4° N geographic, 53.12° N magnetic, and geomagnetic rigidity cutoff 3.6 GV) during a solar flare. An X-ray burst followed by a solar proton event (SPE) resulted in observed changes in the PG and the Jz at ground level and an increase in the ionization in the troposphere [19]. Elhalel et al. [20] investigated the short-term influence of solar disturbances on the fair-weather current (Jz) at the Wise Observatory, Israel, during three solar events—two CMEs and one SEP. The results showed an increase by one order of magnitude in the Jz variance, which was inconclusive since an impact of the local surface wind could not be ruled out (it should be noted that no PG measurements were available at that time). More recently, Tacza et al. [21] measured the effect of solar events on the PG at a low latitude station in Argentina (31.798° S geographic,

21.95° S magnetic, and geomagnetic rigidity cutoff 9.8 GV) and found a noticeably low impact of ~10–15 V m^{-1} variation from fair-weather values.

2. Instrumentation and Observation Sites

In the present study, we rely upon the infrastructure that exists at two measuring sites, and we will review it here briefly. The instruments are located at two permanent sites operated by Tel-Aviv University through collaborative research with Ariel University and Reichman University, Herzliya. The Wise observatory site in Mitzpe Ramon (30°35′ N, 34°45′ E, altitude 850 m above sea level, geomagnetic 27°6′ N 112°23′ E, and geomagnetic rigidity cutoff 10.3 GV) is located near the town Mitzpe Ramon (MR) is an arid plateau in the southern part of Israel (Negev desert). The second site is on Mount Hermon (33°18′ N 35°47.2′ E, altitude of ~2100 m above sea level, geomagnetic 29°36′ N 113°56′ E, and geomagnetic rigidity cutoff 10.1 GV), which is the highest peak in Israel.

Fair-weather ground measurements of the vertical electric field (Ez) have been conducted intermittently since June 2013 and April 2015 at Mitzpe Ramon (MR) and Mount Hermon, respectively. The diurnal fair-weather curves shown in Figure 1 were obtained on dates that are defined meteorologically as fair-weather days. Fair weather in this context is defined as weather with clear skies or a low amount of stratiform clouds (<3/8 cover), wind speed less than 8 m s^{-1} (or less than 30 km h^{-1}), and no precipitation or lightning activity [22]. Throughout the last decade, more capabilities were added to both stations, offering a solid, stable, and clean environment for atmospheric and space weather studies. For observing the vertical component of the atmospheric electric field, we employ the CS110 field mill [23,24]. The vertical conduction current (Jz) in the atmosphere is monitored by the Geometrical Displacement and Conduction Current Sensor (GDACCS) developed at the Meteorology Department of the University of Reading, UK [25]. The mean diurnal PG values for the Wise Observatory are ~150 V/m during local night hours (5–6 UT), reflecting the minimum in the Carnegie curve [26], which is a manifestation of the low lightning activity in the Pacific Ocean. The mean value of the PG increases to ~200 V m^{-1} at local afternoon and early evening hours due to intense lightning activity in the Americas (21 UT), dominating the Carnegie curve [23,24,27]. They found that low clouds, fog, and high humidity and wind speed cause an increase in the measured ground PG at Mitzpe Ramon. The increase can be up to +30 V m^{-1} at times of low clouds and up to +150–300 V m^{-1} at times of fog conditions (high humidity and low wind speed) from fair-weather values.

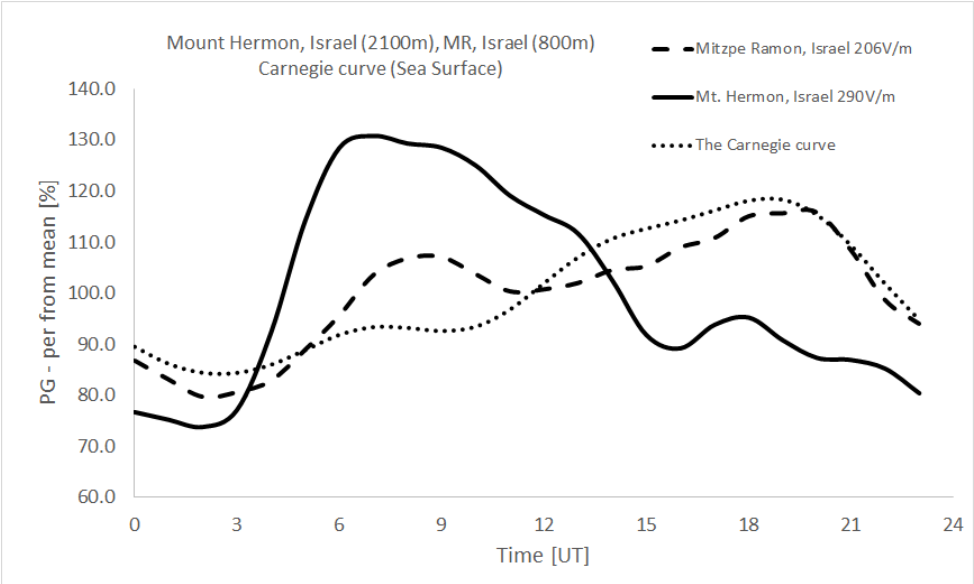

Figure 1. Diurnal fair-weather curves from Mitzpe Ramon [24], Mount Hermon [28], and the Carnegie curve [26].

The mean PG values for Mount Hermon are around 200 V m^{-1} at night hours; the PG then increases to ~360 V m^{-1} during local late morning due to the "Austausch" effect and decreases again to ~260 V m^{-1} in the evening. The stations exhibit ±30 V m^{-1} and ±50 V m^{-1} variations, respectively, around the mean [24]. The mean values of the conduction current density (Jz) measured at Mt. Hermon are in the range of 0.9–1.5 pA m^{-2} and are subjected to daily local variations due to aerosols, wind, and local turbulence, as well as current flowing in the GEC due to global thunderstorm activity [28].

The Israel Cosmic Ray and Space Weather Station on Mt. Hermon measures cosmic ray (CR) fluxes and the specific intensities of neutron multiplicities by using standard 6NM-64 boron trifluoride (BF_3) detectors with an energy threshold of 10.6 GeV. The gamma radiation intensity at ground level is measured by using NaI (Tl) scintillation detectors (PM-11) tuned to the energy range of 50–3000 keV [29,30]. The observatory measures meteorological parameters such as pressure, relative humidity, and temperature as well.

Solar activity, space weather, and their impacts on Earth are monitored by NOAA GOES geostationary satellites (35,786 km altitude). The satellite measures the proton and electron fluxes. The data are plotted in near real-time and presented on the NOAA website (https://www.swpc.noaa.gov/; Accessed 1 August 2023) with an estimated Kp-index (global geomagnetic storm index) bar graph. The list of events such as CMEs, geomagnetic storms, and solar energetic particle (SEP) events detected by the satellites is available on the NOAA website. The parameters (protons and electron flux) measured according to the GOES 13 satellite for the two events are shown in Figures 2a and 3a. We should note that the mean velocity of the solar particles can vary between 300 and 850 km s^{-1} [1,31], resulting in a time delay of 40–70 s between the arrival of the particles to the satellite and when they interact with the Earth's atmosphere.

In order to quantify the contributions of meteorological conditions to the electric parameters measured at the ground, one needs to consider the occurrence of clouds, fog, aerosols, high humidity, and wind speed parameters that were found to affect the local potential gradient [32,33]. For cloudiness data, we used the data archive of the Israeli Meteorological Service (IMS) (https://ims.gov.il/he/data_gov—the data are open to the public, available in Hebrew, and copyrighted to the state of Israel; Accessed 22 July 2023), which provides weather data from Israel, including types of clouds, height of cloud base, and cloud amounts for low, middle, and high clouds in oktas eighths. In addition, we inspected the MODIS infrared and visible Cloud Product data to determine the physical and radiative cloud properties. The data are obtained from the worldview open-source code app website (https://worldview.earthdata.nasa.gov/, Accessed 1 August 2023) and provide interactive browsing for global, full-resolution satellite imagery layers with the availability to download the underlying data. The AERONET (AErosol RObotic NETwork) project is an array of ground-based remote sensing aerosol networks established by NASA that provides globally distributed observations of spectral aerosol optical depth (AOD). The station we obtained the data from is located in Sde Boker, southern Israel (30.855° N, 34.782° E), approximately 20 km north of the Wise Observatory. Previous studies found that the range of fair-weather mean AOD value at Mitzpe Ramon ranges from 0.17 to 0.3 [23,24]. Finally, we used local meteorological stations at both sites to obtain weather parameters such as relative humidity, pressure, temperature, and wind speed.

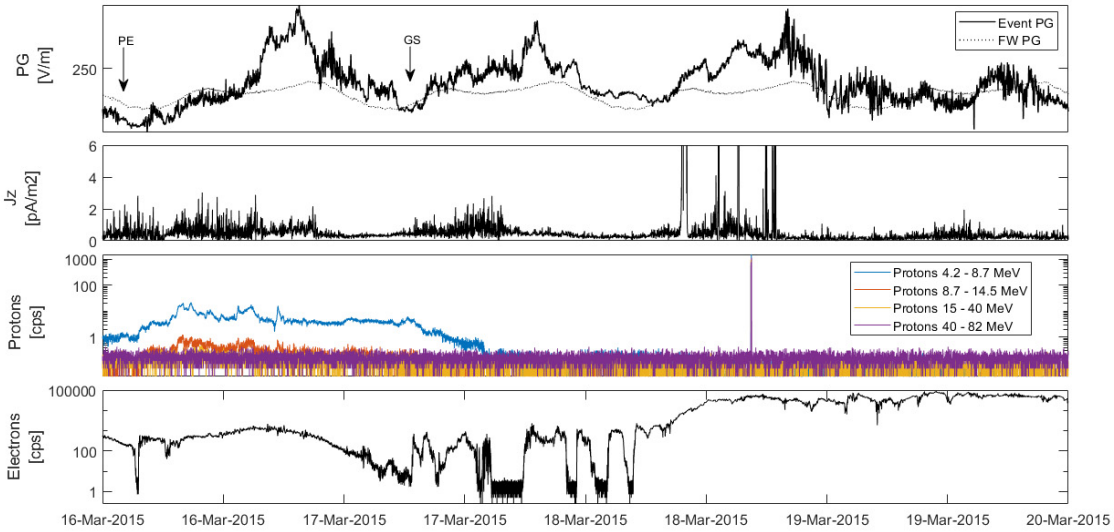

(**a**)

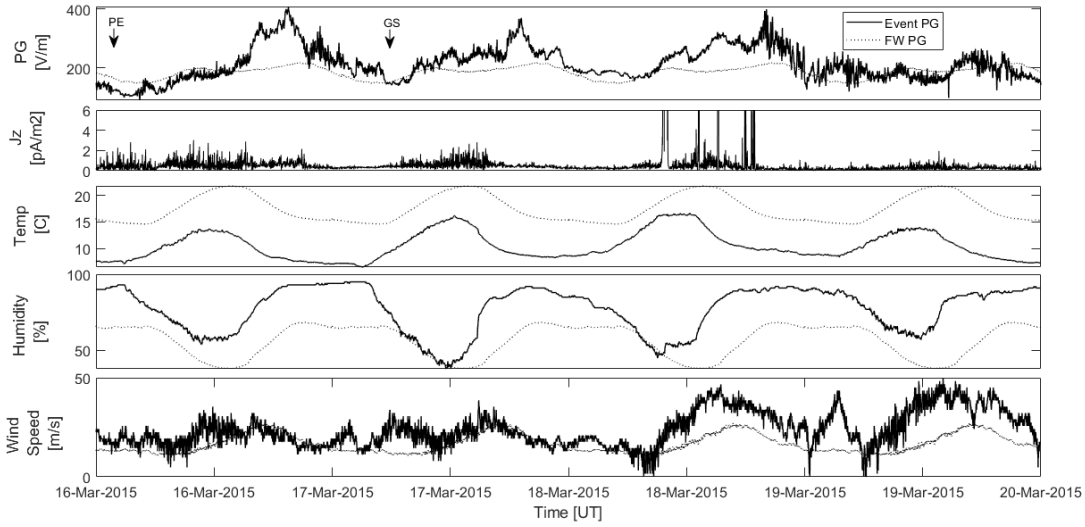

(**b**)

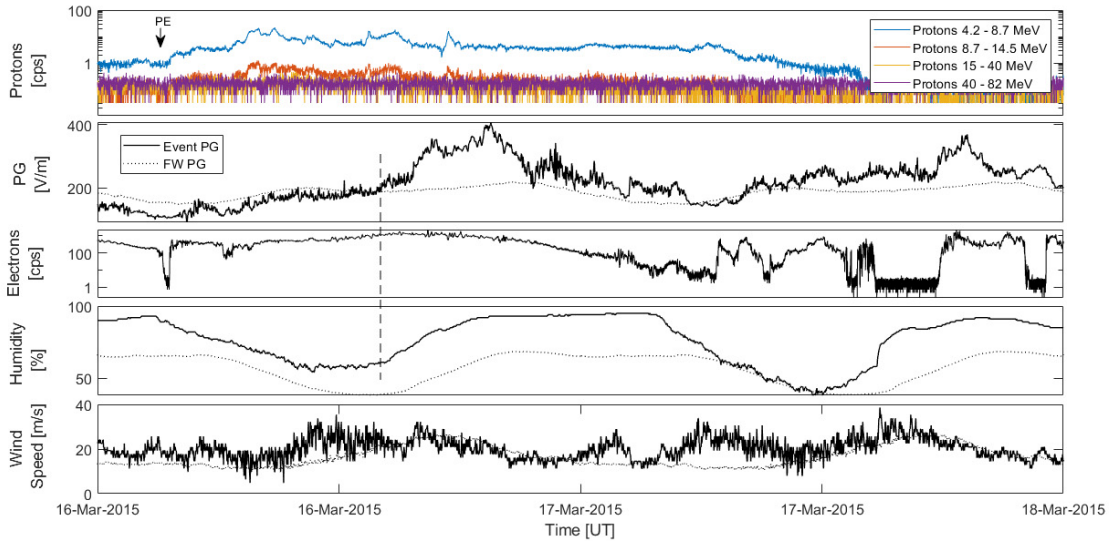

(**c**)

Figure 2. *Cont.*

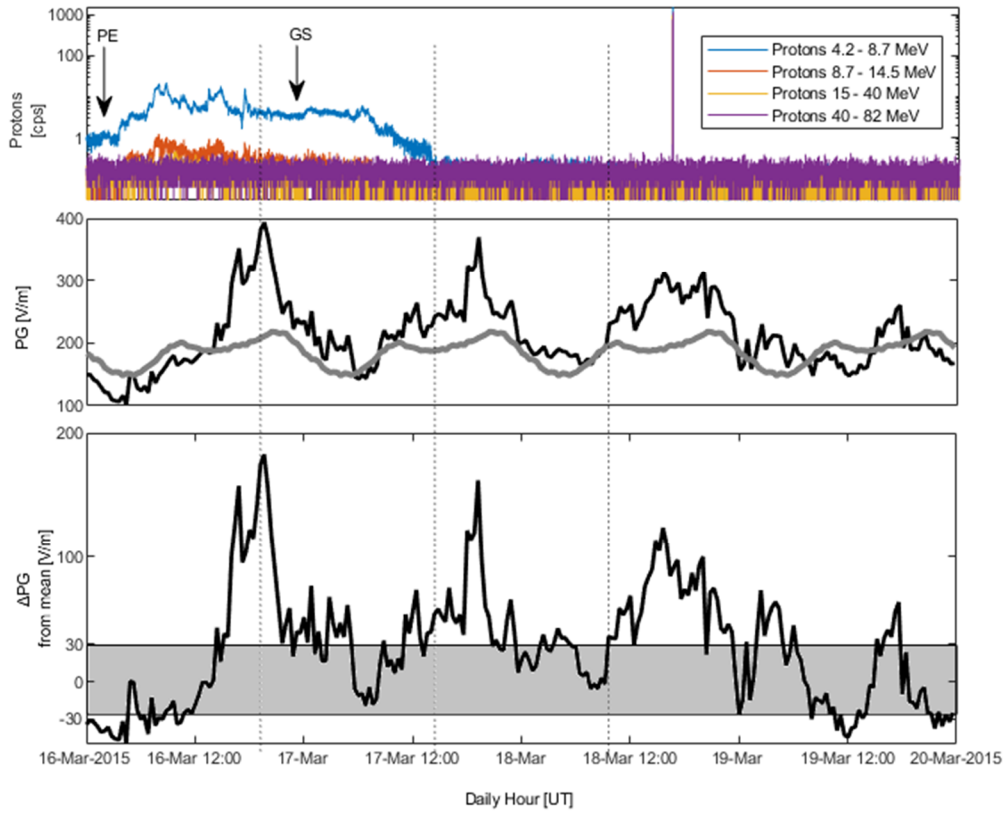

(**d**)

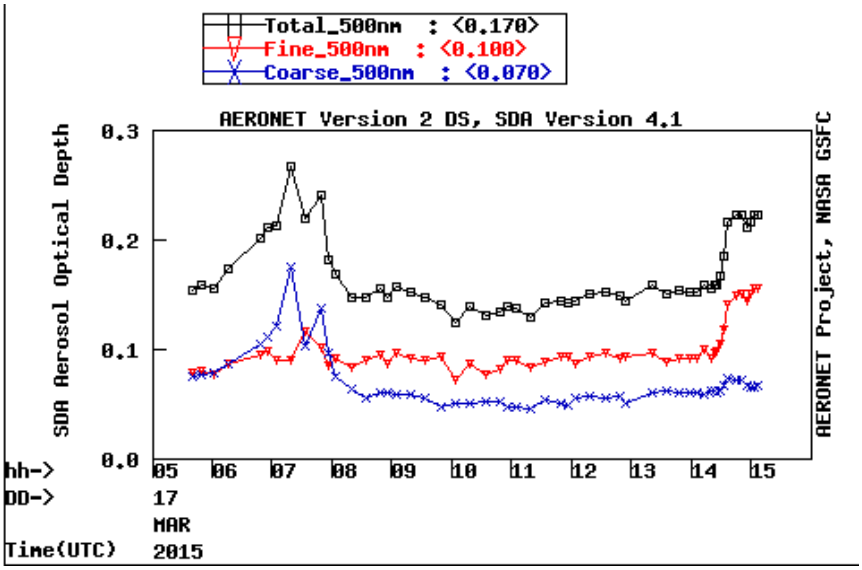

(**e**)

Figure 2. (**a**) Mitzpe Ramon station parameters on 16–20 March 2015: PG (top panel), Jz (second panel), and the satellite environment measured by GOES 13—proton and electron flux (bottom panels). The temporal resolution is 1 min. (**b**) Mitzpe Ramon station parameters on 16–20 March 2015: PG (top panel), conduction current Jz (second panel), and meteorological parameters of temperature, humidity, and wind speed (bottom three panels). Dotted lines are mean patterns of fair-weather behavior. PE stands for the start of the proton event, and GS is the start of the geomagnetic storm. Temporal resolution is 1 min. (**c**) Mitzpe Ramon station zoom-in on the solar event from 16 March 00:00 to 18 Mar 00:00—the parameters are protons and electron flux, PG, humidity, and wind speed. Dashed line represents the time when humidity starts to increase. Temporal resolution is 1 min.

(**d**) ΔPG analysis. The solar proton flux with event time indication (top), PG values in black during the event compared to the fair-weather Ramon curve in grey (middle), ΔPG and standard deviation grayed area that show diurnal fair-weather variations from the Ramon station (bottom). (**e**) Sat image of Israel from 17 Mar 2015 showing scattered low clouds in central and northern regions and no clouds at all in the southern region. Black dot is the MR station (left). Daily average of fine and coarse particles AOD on 17 Mar 2015 (right). The red curve is the fine-mode AOD at 500nm which represents the attenuation of light due to smaller aerosol particles (less than 2.5 micrometers) at a wavelength of 500 nanometers. The blue curve is the coarse-mode AOD at 500nm for larger aerosol particles with diameters greater than 2.5 micrometers. The black line is the total of both.

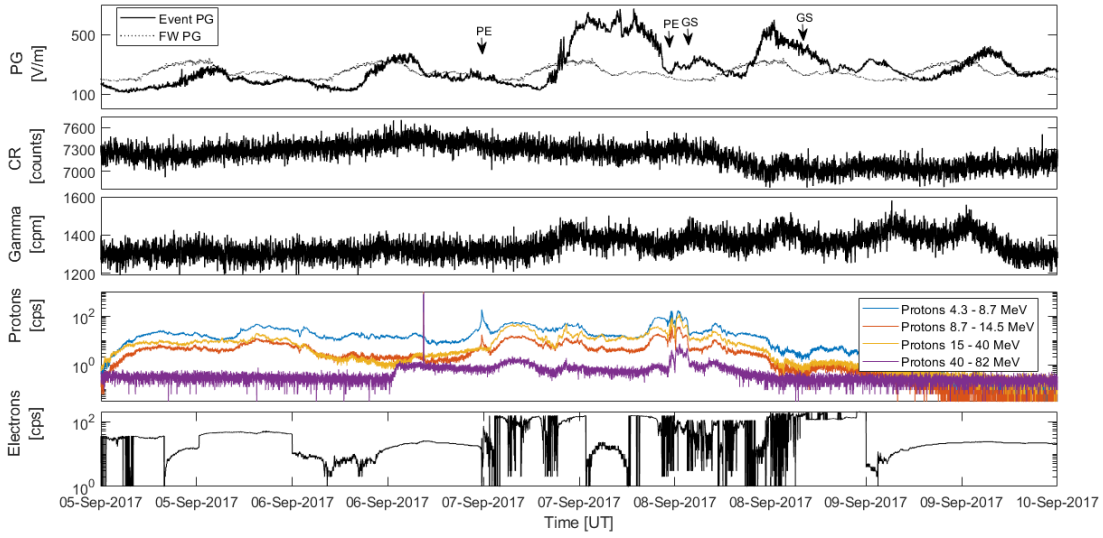

(**a**)

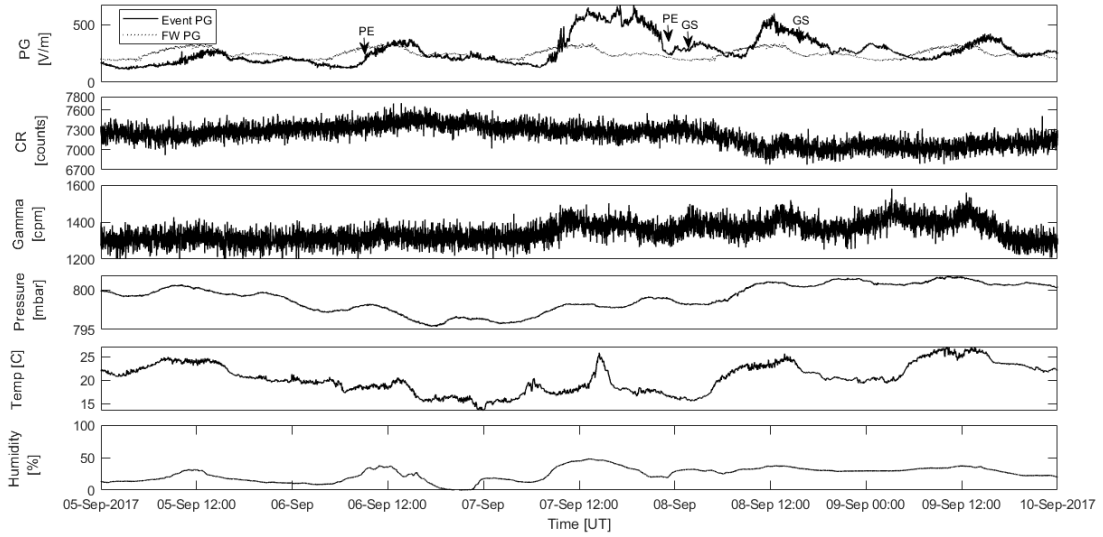

(**b**)

Figure 3. *Cont.*

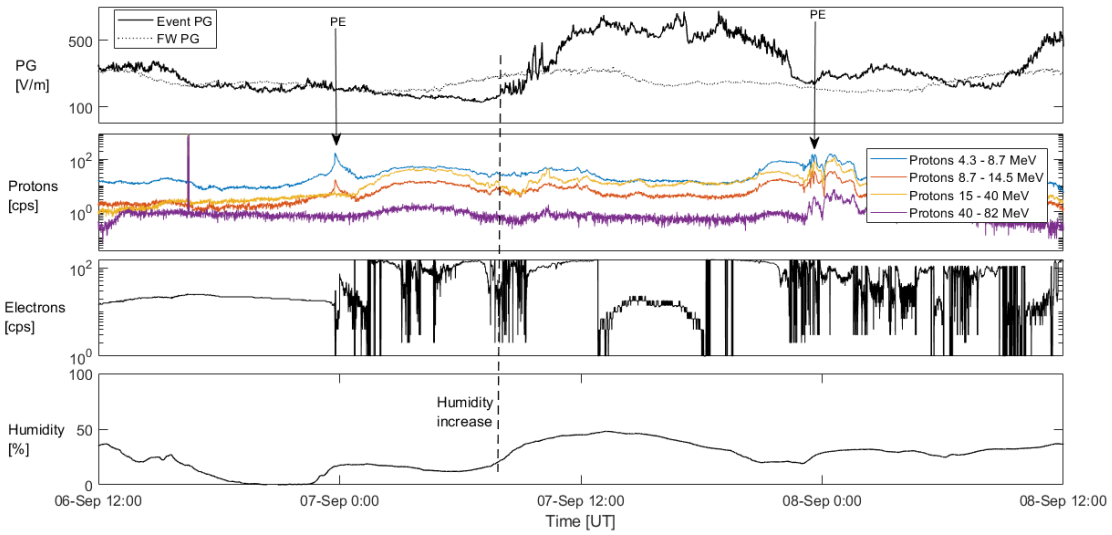

(**c**)

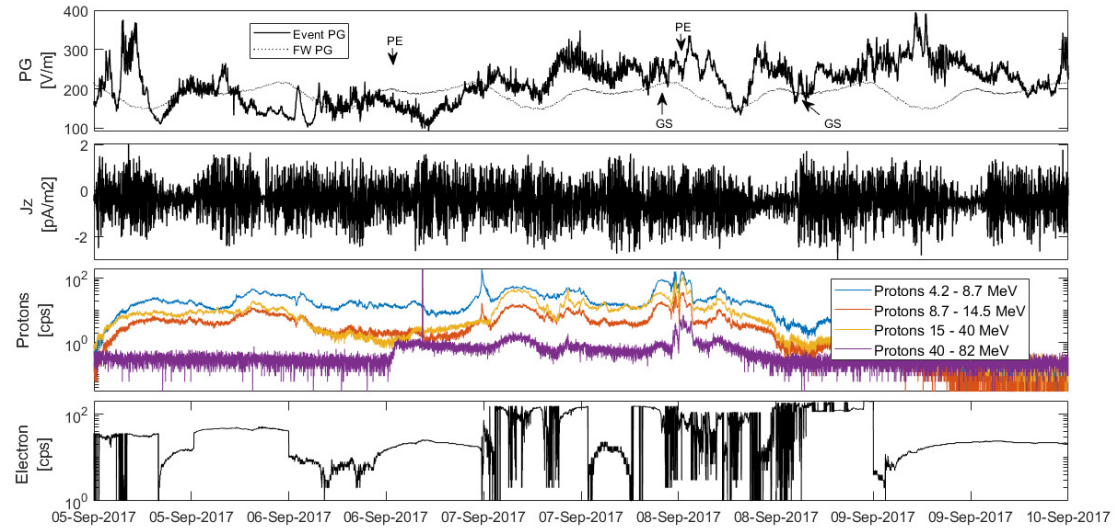

(**d**)

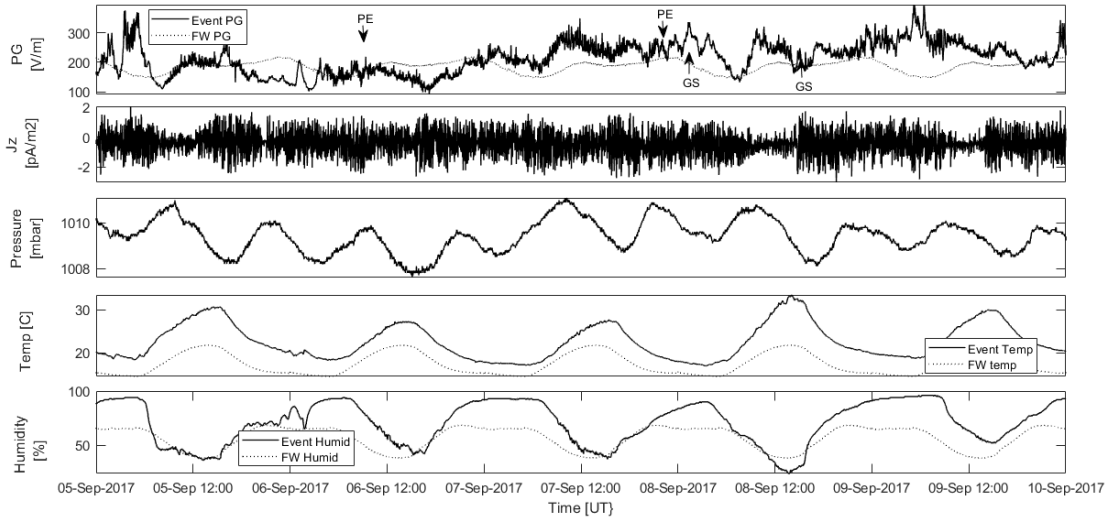

(**e**)

Figure 3. *Cont.*

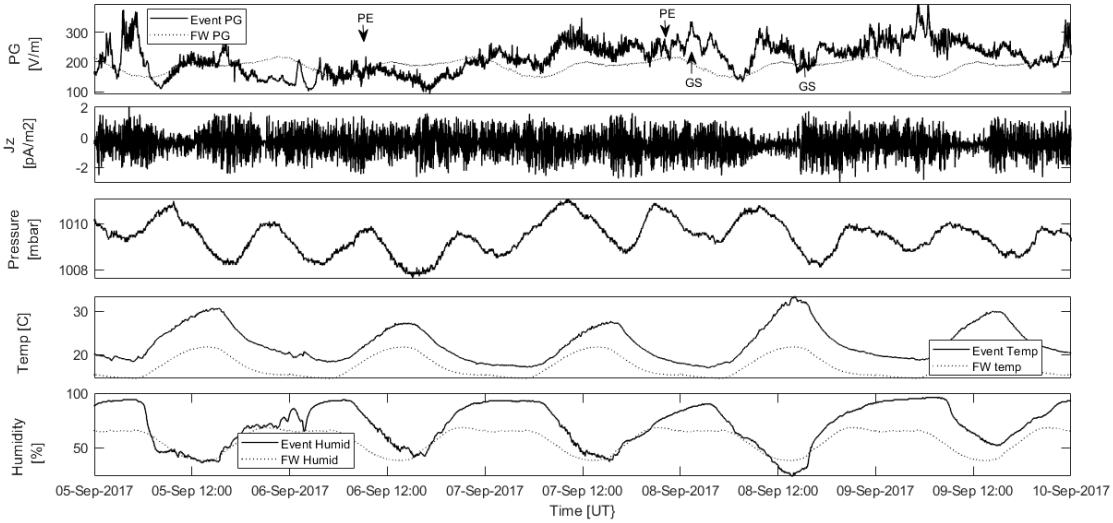

(**f**)

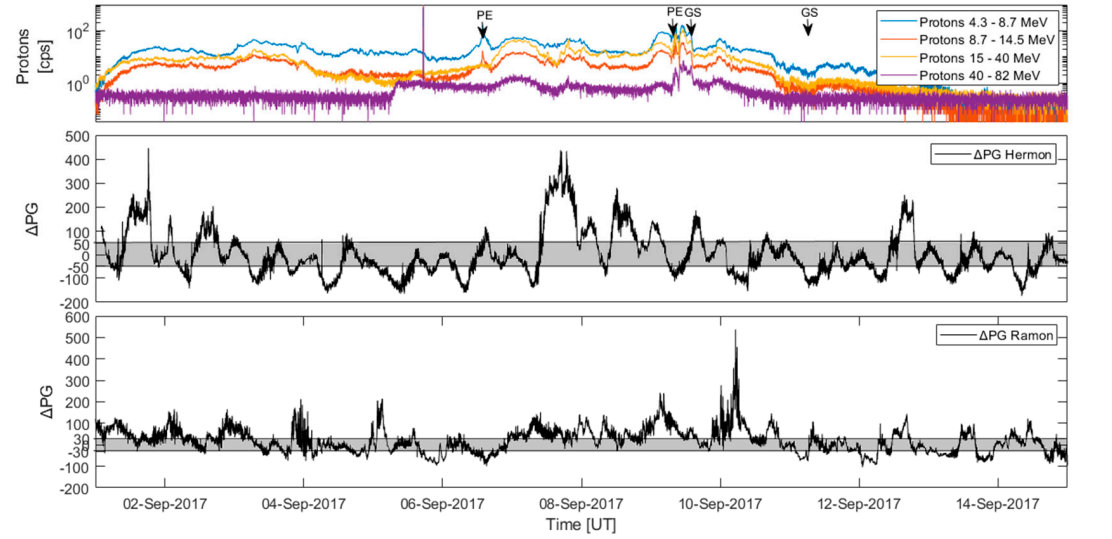

(**g**)

Figure 3. *Cont.*

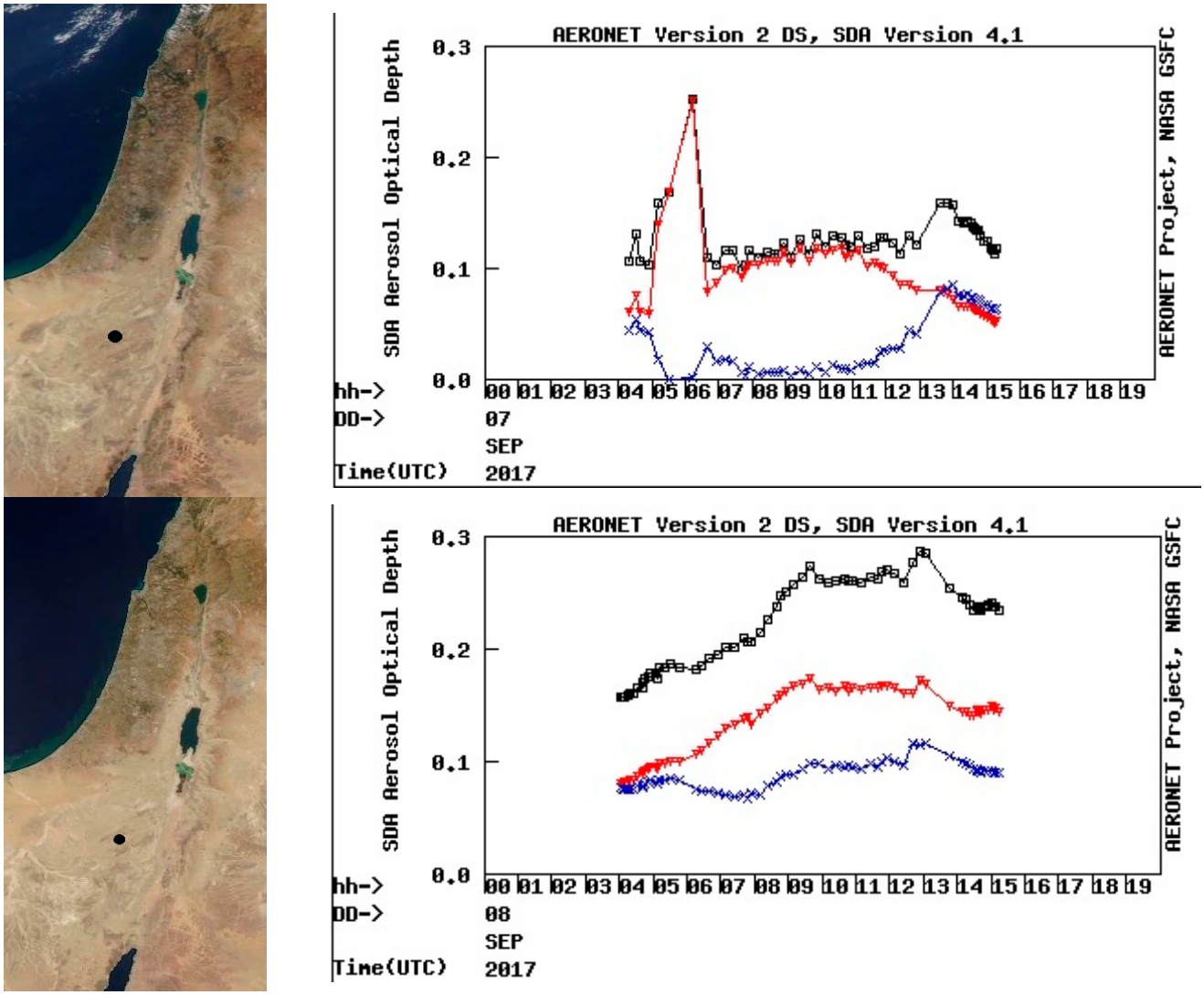

(**h**)

Figure 3. (**a**) Mt. Hermon station parameters on 5–10 September 2017: PG (top panel), cosmic ray intensity counts (second panel), Gamma detectors (third panel), and the satellite environment measured by GOES 13—proton and electron flux (bottom panels). The temporal resolution is 1 min. (**b**) Mt. Hermon station parameters on 5–10 September 2017: PG (top panel), cosmic ray intensity counts (second panel), Gamma detectors (third panel), and meteorological parameters of pressure, temperature, and humidity (bottom three panels). Dotted lines are mean patterns of fair-weather behavior. PE stands for the start of the proton event, and GS is the start of the geomagnetic storm. The temporal resolution is 1 min. (**c**) Mt. Hermon station zoom-in on the solar event—the parameters presented are as follows: proton and electron fluxes, PG, and humidity values. Dashed line represents the time when humidity starts to increase. The temporal resolution is 1 min. (**d**) Mitzpe Ramon station parameters on 5–10 September 2017: PG (top panel), conduction current Jz (second panel), and meteorological parameters of pressure, temperature, and humidity (bottom three panels). Dotted line shows the mean pattern of fair-weather behavior. PE stands for the start of the proton event, and GS is the start of the geomagnetic storm. The temporal resolution is 1 min. (**e**) Mitzpe Ramon station parameters on 5–10 September 2017: PG (top panel), conduction current Jz (second panel), and the satellite environment measured by GOES 13—proton and electron flux (bottom panels). The temporal resolution is 1 min. (**f**) Mitzpe Ramon station zoom-in on the solar event—the parameters shown are as follows: proton and electron fluxes, PG, and humidity values. Dashed line represents the time when humidity starts to increase. The temporal resolution is 1 min. (**g**) ΔPG analysis. The

solar proton flux with event time is indicated by arrows (top), ΔPG, and standard deviation grayed area that show diurnal fair-weather variations from the Hermon station (middle) and the Ramon station (bottom). (**h**) Satellite image of Israel showing no clouds at all in the southern region (black dot denotes the MR station) with daily average of fine and coarse particles AOD from 7 September 2017 (top) and 8 September 2017 (bottom). The red curve is the fine-mode AOD at 500nm which represents the attenuation of light due to smaller aerosol particles (less than 2.5 micrometers) at a wavelength of 500 nanometers. The blue curve is the coarse-mode AOD at 500nm for larger aerosol particles with diameters greater than 2.5 micrometers. The black line is the total of both.

3. Results

Here, we present two case studies, which are considered the strongest of the >25 solar events that occurred during the study period (2012–2017). That period coincided with the end of the maximum of solar cycle 24 and the decline period toward the solar minimum in 2019–2020. We show the variations of the PG, Jz, CR, gamma ray intensity, and the meteorological data before, during, and after the impact of the solar energetic particle (SEP) events on Earth's magnetic field in search for anomalies that can be attributed to electrical changes in the GEC. In addition, we zoom in on the period of the day of the event to detect in more detail possible changes in the above-mentioned parameters and plot the difference (ΔPG) between fair-weather patterns to PG values measured during a geomagnetic storm induced by a solar event. The start of each event (SEP or geomagnetic storms) caused by a solar event is marked on the graphs by black arrows and designations for "PE" and "GS" for the proton event and geomagnetic storms, respectively. All the times referred to in the figures are UT. Finally, we will try to investigate the contributions, if any were present during the case studies, of other factors (e.g., clouds, fog, and aerosols) to rule out or understand the combined effects on the PG.

3.1. St. Patrick's Day CME Event 16–20 March 2015

The St. Patrick's Day solar storm had a maximum Kp index = 9, making it the strongest event of 2015. The storm produced a solar proton event from March 16th, followed by a strong CME event that arrived at Earth on the morning of 17 March and lasted for more than 24 h, causing strong disturbances that were measured by the GOES13 satellite (Figure 2a).

The variations in the proton flux were followed by strong variations in the electron flux, which reached peak values in the midday of 17 March 2015 when the estimated Kp index reached level 9. Figure 2b shows ground measurements of the PG, Jz, and meteorological data from Mitzpe Ramon (unfortunately, due to technical problems, the Mt. Hermon station was out of order during this event). A slight increase in the PG above mean fair-weather values was observed during the midnight hours of 16 March, increasing to 430 V m^{-1} before reverting back to fair-weather values. Throughout this event, the conduction current values fluctuated between 1 and 3 pA m^{-2}. A period with a large variation of the conduction current exhibiting values of ~400 pA m^{-2} was recorded on 18 March between 12 and 18 UT. The episode was accompanied by an increase in the potential gradient. The values of temperature, relative humidity, and wind speed were higher than the typical pattern of mean fair-weather behavior (e.g., the wind speed was up to 50 km h^{-1}, which is much higher than the limit of <30 km h^{-1} of the fair-weather criteria [22]). The PG and Jz disturbances occurred during the same period of time of high relative humidity and strong wind, indicating that the source of fluctuation may be related to local weather patterns, which obscured the solar signal, if it existed at all. On the other hand, the relative humidity and high wind speed values do not imply conditions to generate fog; thus, we can negate the PG increase due to the presence of fog [27].

Figure 2c is a zoom-in of the event and shows that there is a slight increase in the PG when the proton flux increases, but the high values and the response above fair-weather values begin several hours after the start of the event and are not immediate (or at least with a 70 s delay) as would have been expected compared to past results [16]. The dashed

line shows that the increase in the PG also occurred at the same time as an increase in the humidity, as reported recently by Yair and Yaniv (2023).

The PG values return to slightly above fair-weather values when the humidity decreases, and they rise again when there is a renewed increase in humidity, as expected from the weather-controlled daily cycle [24]. The ΔPG analysis (Figure 2d) reveals a difference of +30–200 V m^{-1} above fair-weather values several hours after the proton event, a fact that supports the idea of PG response due to local meteorological effects. No clouds were observed in satellite images (Figure 2e) above the Mitzpe Ramon station at the time of the solar event, negating the factor of PG variability due to clouds. Aerosol concentration analysis (AOD) at the region during the solar events found values of 0.05–0.25, which correspond to fair-weather values [23], negating the potential contribution of high aerosol concentrations.

3.2. CME Event 6–8 September 2017

This solar event was the strongest event of 2017 and the 12th strongest event to date to be recorded by NASA. In this event, the sun produced several CMEs and SF in succession in a few days, creating very complex space weather conditions in the heliosphere Figure 3a shows 5 days of space weather data from 5 to 10 September 2017 and the strong CME, which erupted from the sun on 6 September 2017, reaching Earth on 8 September with high proton and electron fluxes. The Kp values were above 6, reaching a maximum value of Kp = 9 throughout 8 September. The 10 MeV proton flux was high (50–100 cps) during the entire period, and high energy proton fluxes (up to 10 cps) of 50 and 100 MeV were measured on 6 September 2017 at 12UT. Both our stations recorded continuous PG data, and below, we review them and compare them with space weather parameters.

Figure 3a,b presents the PG variations from the Mt. Hermon station (bold black) and the fair-weather PG behavior (black dotted line). The PG values show a clear increase of 150–250 V m^{-1} around 7 September 12 UT. Sadly, the Mt. Hermon Jz station suffered from internal noise, and the data was not retrievable. The second panel of Figure 3a shows (pressure-corrected) CR counts from Mt. Hermon and exhibits a continuing decrease over a period of several hours of ~400 counts, which constitute ~5% of the counts before the event, indicating a minor Forbush decrease. We should note that cosmic ray data from Mt. Hermon station exhibit a regular daily variation of 0.5–1% when space weather conditions are quiet [34]); therefore, a 5% decrease clearly suggests a Forbush decrease from a solar event. This FD was also detected around the world with other NM but also with muon stations, for example, at Oulu, Finland [35] and Belgrade, Serbia [36].

The gamma detector on Mt. Hermon (third panel in Figure 3a) showed an increase of 10–15% (150–200 cpm higher) starting from 7 September and throughout the following day. The bottom three panels in Figure 3b show the meteorological data on the mountain, exhibiting values slightly above the average fair-weather values (30% humidity; [12]. It should be noted that no wind data were available during the event. Figure 3c is a zoom-in on the event, which shows that the increase in the PG correlates with the time of increase in the relative humidity, suggesting a higher concentration of water vapor and a decrease in conductivity followed by an increase in the PG, as measured by Bennet and Harrison [32]. We can rule out the possibility that the change is related to the incoming particle flux since there was an apparent response of the PG to the humidity increase several hours after the event (marked as PE on Figure 3b) on the 6th or to the electron flux (marked as GS on Figure 3b) on 8 September. The diurnal pattern of the PG at the Hermon station with the "Austausch" effect continued as usual despite this strong space weather event [24].

Figure 3d,e presents the PG variations for the same period of time detected at the Wise Observatory station (bold black) as well as the average fair-weather PG behavior (black dotted line). The Mitzpe Ramon station shows an increase of ~50–150 V m^{-1} compared with fair-weather values. The Jz data showed no significant departures from fair-weather values and fluctuated between ~±2 pA m^{-2}. The relative humidity showed values above the average, up to 90–100%, that persisted from local evening until noon hours. Such a high humidity indicates fog conditions [27]. We observe no conspicuous response of the PG

to the increase in the low energy proton flux (marked as PE in Figure 3a) on 6 September. Similar to the Mt. Hermon results, Figure 3f shows a zoom-in on the event, which shows that the values of PG are higher (50–250 V m^{-1}) than the fair-weather values during and after the event compared to the days before the event. The ΔPG analysis (Figure 2d) exhibits a difference of +50–250 V m^{-1} and +30–150 V m^{-1} above fair-weather values several hours after the proton event at both Mt. Hermon and Ramon stations (respectively), suggesting that, again, the source of the delayed PG response is a superposition of local meteorological effects, especially high humidity.

No clouds were observed by satellite images from 7 and 8 September 2017 (Figure 3h top and bottom) above the Mitzpe Ramon at the time of the solar event, negating the factor of PG increase due to low clouds. Aerosol analysis (AOD) at the region during the solar events found AOD values below 0.3, which are fair-weather values according to previous studies [23,24], negating any PG increase that might result from a high aerosol concentrations.

4. Summary

Two case studies of unusually strong solar proton events accompanied by geomagnetic storms impacting Earth's atmosphere were analyzed in search of a response to parameters of the global electric circuit at two low-latitude stations in Israel. The 2015 St. Patrick's Day event (case study 1) was an SEP followed by a strong geomagnetic storm of Kp = 9, and the one on 6–8 September 2017 had also reached a maximum of Kp = 9.

Our analysis ruled out the possibility that the observed PG increase was due to the presence of clouds and high concentrations of aerosols. Still, it is likely that the observed increase in the potential gradient and current density during both case studies can be explained by local temporal meteorological conditions, probably high humidity and strong winds. The high relative humidity can lead to the formation of small droplets and hydrated ion clusters, which reduces atmospheric conductivity [27,32]. The strong wind that was measured (~30–50 km h^{-1}) can transport aerosols and space charge, thus affecting the local resistivity, the ambient electric field, and current density [37,38]. Both meteorological effects lower the conductivity and increase the PG, as required by Ohm's law.

The results from the Israeli stations do not agree with past observations [17–19] that showed an increase in the surface electric field during and after SEP events and geomagnetic storms. We should note an important difference between these observations, stemming from the fact that the majority of past results were obtained at higher latitudes >45° N, which naturally have lower cutoff rigidity values (~3 GV and lower) where the magnetospheric shielding is less intense, compared to the 10.3 GV at the latitudes of Israel, ~30° N [39]. A similar low latitude station in Argentina (9.8 GV cutoff rigidity) shows that the impact on the PG was found to be of the order of ~10–15 V m^{-1} [40], an almost negligible offset that can be easily masked by local meteorological conditions [41]. Based on the known variations of the fair-weather potential gradient of ±30 V m^{-1} and ±50 V m^{-1} at Mitzpe Ramon and Mt. Hermon, respectively, our results suggest that ionization effects and PG changes due to strong solar events were entirely masked and were below the detection threshold [42,43], and thus could not be observed in the geographical latitudes of Israel. A possible interpretation of the results suggests that even the strongest solar events that generate geomagnetic storms with electron fluxes (~1 MeV) and solar energetic particle events (proton fluxes higher than 10 Mev) are effectively shielded at low latitudes (30° N), such as the locations of our two stations in Israel. This shielding precludes the appearance of significant signals in the ambient electric field at the surface level that may be conspicuous above the normal fair-weather fluctuations, which are always dominated by local daily meteorological factors, such as high humidity and wind.

Author Contributions: Conceptualization, R.Y. and Y.Y.; Validation, C.P.; Formal analysis, R.Y.; Resources, Y.Y.; Data curation, R.Y. and Y.R.; Writing—original draft, R.Y.; Writing—review & editing, Y.Y., C.P. and Y.R.; Supervision, C.P.; Funding acquisition, Y.Y. All authors have read and agreed to the published version of the manuscript.

Funding: No funding was received.

Institutional Review Board Statement: Not applicable.

Informed Consent Statement: Not applicable.

Data Availability Statement: The Potential Gradient data (PG) is available through the GLOCAEM network at U. Reading, UK: https://catalogue.ceda.ac.uk/uuid/bffd0262439a4ecb8fadf0134c4a4a41.

Acknowledgments: This research was supported by the Israel Science Foundation (grant No. 423/14). We thank Lev Pustilnik for his help with the Cosmic Ray data from Mt. Hermon and Sami Ben-Gigi for helping with the Wise Observatory station. The sunspot number data are taken from SILSO data/image, Royal Observatory of Belgium, Brussels. NOAA GOES data are from http://www.swpc.noaa.gov.

Conflicts of Interest: The authors declare no conflict of interest.

References

1. Rycroft, M.J.; Israelsson, S.; Price, C. The global atmospheric electric circuit, solar activity and climate change. *J. Atmos. Sol.-Terr. Phys.* **2000**, *62*, 1563–1576. [CrossRef]
2. Liu, J.; Wang, W.; Qian, L.; Lotko, W.; Burns, A.G.; Pham, K.; Lu, G.; Solomon, S.C.; Liu, L.; Wan, W.; et al. Solar flare effects in the Earth's magnetosphere. *Nat. Phys.* **2021**, *17*, 807–812. [CrossRef]
3. Rycroft, M.J.; Nicoll, K.A.; Aplin, K.L.; Harrison, R.G. Recent advances in global electric circuit coupling between the space environment and the troposphere. *J. Atmos. Sol.-Terr. Phys.* **2012**, *90*, 198–211. [CrossRef]
4. Mironova, I.A.; Aplin, K.L.; Arnold, F.; Bazilevskaya, G.A.; Harrison, R.G.; Krivolutsky, A.A.; Nicoll, K.A.; Rozanov, E.V.; Turunen, E.; Usoskin, I.G. Energetic particle influence on the Earth's atmosphere. *Space Sci. Rev.* **2015**, *194*, 1–96. [CrossRef]
5. Zhao, L.L.; Zhang, H. Transient galactic cosmic-ray modulation during solar cycle 24: A comparative study of two prominent Forbush decrease events. *Astrophys. J.* **2016**, *827*, 13. [CrossRef]
6. Usoskin, I.G.; Desorgher, L.; Velinov, P.; Storini, M.; Flückiger, E.O.; Bütikofer, R.; Kovaltsov, G.A. Ionization of the earth's atmosphere by solar and galactic cosmic rays. *Acta Geophys.* **2009**, *57*, 88–101. [CrossRef]
7. Bazilevskaya, G.A.; Usoskin, I.G.; Flückiger, E.O.; Harrison, R.G.; Desorgher, L.; Bütikofer, R.; Krainev, M.B.; Makhmutov, V.S.; Stozhkov, Y.I.; Svirzhevskaya, A.K.; et al. Cosmic Ray Induced Ion Production in the Atmosphere. *Space Sci. Rev.* **2008**, *137*, 149–173. [CrossRef]
8. Haldoupis, C.; Rycroft, M.; Williams, E.; Price, C. Is the "Earth-ionosphere capacitor" a valid component in the atmospheric global electric circuit? *J. Atmos. Sol.-Terr. Phys.* **2017**, *164*, 127–131. [CrossRef]
9. Kasatkina, E.A.; Shumilov, O.I.; Rycroft, M.J.; Marcz, F.; Frank-Kamenetsky, A.V. Atmospheric electric field anomalies associated with solar flare/coronal mass ejection events and solar energetic charged particle "Ground Level Events". *Atmos. Chem. Phys. Discuss.* **2009**, *9*, 21941–21958.
10. Holzworth, R.H. High latitude stratospheric electrical measurements in fair and foul weather under various solar conditions. *J. Atmos. Terr. Phys.* **1981**, *43*, 1115–1125. [CrossRef]
11. Holzworth, R.H.; Norville, K.W.; Williamson, P.R. Solar flare perturbations in stratospheric current systems. *Geophys. Res. Lett.* **1987**, *14*, 852–855. [CrossRef]
12. Nikiforova, N.N.; Kleimenova, N.G.; Kozyreva, O.V.; Kubitski, M.; Michnowski, S. Unusual variations in the atmospheric electric field during the main phase of the strong magnetic storm of October 30, 2003, at Swider Polish midlatitude observatory. *Geomagn. Aeron.* **2005**, *45*, 140–144.
13. Tinsley, B.A. Correlations of atmospheric dynamics with solar wind-induced changes of air-Earth current density into cloud tops. *J. Geophys. Res. Atmos.* **1996**, *101*, 29701–29714. [CrossRef]
14. Cobb, W.E. Evidence of a solar influence on the atmospheric electric elements at Mauna Loa Observatory. *Mon. Weather Rev.* **1967**, *95*, 905–911. [CrossRef]
15. Reiter, R. Solar flares and their impact on potential gradient and air-earth current characteristics at high mountain stations. *Pure Appl. Geophys.* **1969**, *72*, 259–267. [CrossRef]
16. Sheftel, V.M.; Bandilet, O.I.; Yaroshenko, A.N.; Chernyshev, A.K. Space-time structure and reasons of global, regional, and local variations of atmospheric electricity. *J. Geophys. Res. Atmos.* **1994**, *99*, 10797–10806.
17. Kleimenova, N.; Kozyreva, O.; Kubicki, M.; Michnowski, S. Variations of the mid-latitude atmospheric electric field (Ez) associated with geomagnetic disturbances and Forbush decreases of cosmic rays. *Recent Dev. Atmos. Electr. Publs. Inst. Geophys. Pol. Acad. Sci.* **2009**, *412*, 55–64.
18. Smirnov, S. Reaction of electric and meteorological states of the near-ground atmosphere during a geomagnetic storm on 5 April 2010. *Earth Planets Space* **2014**, *66*, 5. [CrossRef]
19. Nicoll, K.A.; Harrison, R.G. Detection of lower tropospheric responses to solar energetic particles at midlatitudes. *Phys. Rev. Lett.* **2014**, *112*, 225001. [CrossRef]

20. Elhalel, G.; Yair, Y.; Nicoll, K.; Price, C.; Reuveni, Y.; Harrison, R.G. Influence of short-term solar disturbances on the fair weather conduction current. *J. Space Weather Space Clim.* **2014**, *4*, A26. [CrossRef]
21. Tacza, J.; Raulin, J.P.; Mendonca, R.R.S.; Makhmutov, V.S.; Marun, A.; Fernandez, G. Solar effects on the atmospheric electric field during 2010–2015 at low latitudes. *J. Geophys. Res. Atmos.* **2018**, *123*, 11–970. [CrossRef]
22. Harrison, R.G.; Nicoll, K.A. Fair weather criteria for atmospheric electricity measurements. *J. Atmos. Sol.-Terr. Phys.* **2018**, *179*, 239–250. [CrossRef]
23. Yaniv, R.; Yair, Y.; Price, C.; Katz, S. Local and global impacts on the fair-weather electric field in Israel. *Atmos. Res.* **2016**, *172*, 119–125. [CrossRef]
24. Yaniv, R.; Yair, Y.; Price, C.; Mkrtchyan, H.; Lynn, B.; Reymers, A. Ground-based measurements of the vertical E-field in mountainous regions and the "Austausch" effect. *Atmos. Res.* **2017**, *189*, 127–133. [CrossRef]
25. Bennett, A.J.; Harrison, R.G. Surface measurement system for the atmospheric electrical vertical conduction current density, with displacement current density correction. *J. Atmos. Sol.-Terr. Phys.* **2008**, *70*, 1373–1381. [CrossRef]
26. Harrison, R.G. The carnegie curve. *Surv. Geophys.* **2013**, *34*, 209–232. [CrossRef]
27. Yair, Y.; Yaniv, R. The effects of fog on the atmospheric electrical field close to the surface. *Atmosphere* **2023**, *14*, 549. [CrossRef]
28. Yaniv, R.; Reuveni, Y.; Yair, Y.; Lynn, B. Temporal variations of the conduction current density during fair weather days in Israel. *Atmos. Res.* **2019**, *222*, 1–11. [CrossRef]
29. Reuveni, Y.; Price, C. A new approach for monitoring the 27-day solar rotation using VLF radio signals on the Earth's surface. *J. Geophys. Res. Space Phys.* **2009**, *114*, A10306. [CrossRef]
30. Reuveni, Y.; Yair, Y.; Price, C.; Steinitz, G. Ground level gamma-ray and electric field enhancements during disturbed weather: Combined signatures from convective clouds, lightning and rain. *Atmos. Res.* **2017**, *196*, 142–150. [CrossRef]
31. Kallenrode, M.B. *Space Physics: An Introduction to Plasmas and Particles in the Heliosphere and Magnetospheres*, 3rd ed.; Springer: Berlin/Heidelberg, Germany, 2004; p. 374.
32. Bennett, A.J.; Harrison, R.G. Atmospheric electricity in different weather conditions. *Weather* **2007**, *62*, 277–283. [CrossRef]
33. Yaniv, R.; Yair, Y. Electric Field Variations Caused by Low, Middle and High-Altitude Clouds over the Negev Desert, Israel. *Atmosphere* **2022**, *13*, 1331. [CrossRef]
34. Dorman, L. *Cosmic Rays in the Earth's Atmosphere and Underground*; Springer Science & Business Media: New York, NY, USA, 2013; Volume 303.
35. Badruddin, B.; Aslam, O.P.M.; Derouich, M.; Asiri, H.; Kudela, K. Forbush decreases and geomagnetic storms during a highly disturbed solar and interplanetary period, 4–10 September 2017. *Space Weather* **2019**, *17*, 487–496. [CrossRef]
36. Savić, M.; Veselinović, N.; Dragić, A.; Maletić, D.; Joković, D.; Banjanac, R. Rigidity dependence of Forbush decreases in the energy region exceeding the sensitivity of neutron monitors. *Ad. Sp. Res.* **2019**, *63*, 1483–1489. [CrossRef]
37. Yair, Y.; Levin, Z. Charging of polydispersed aerosol particles by attachment of atmospheric ions. *J. Geophys. Res.* **1989**, *94*, 13085–13091. [CrossRef]
38. Lucas, G.M.; Thayer, J.P.; Deierling, W. Statistical analysis of spatial and temporal variations in atmospheric electric fields from a regional array of field mills. *J. Geophys. Res. Atmos.* **2017**, *122*, 1158–1174. [CrossRef]
39. Makhmutov, V.; Bazilevskaya, G.; Stozhkov, Y.; Philippov, M.; Yair, Y.; Yaniv, R.; Harrison, G.; Nicoll, K.; Aplin, K. Cosmic ray measurements in the atmosphere at several latitudes in October 2014. In Proceedings of the 34th International Cosmic Ray Conference, The Hague, The Netherlands, 30 July–6 August 2015.
40. Tacza, J.; Raulin, J.-P.; Macotela, E.; Norabuena, E.; Fernandez, G.; Correia, E.; Rycroft, M.; Harrison, R. A new South American network to study the atmospheric electric field and its variations related to geophysical phenomena. *J. Atmos. Sol.-Terr. Phys.* **2014**, *120*, 70–79. [CrossRef]
41. Harrison, R.G. Columnar resistance changes in urban air. *J. Atmos. Sol.-Terr. Phys.* **2005**, *67*, 763–773. [CrossRef]
42. Qiu, S.; Xie, Y.; Shi, M.; Yousof, H.; Soon, W.; Ren, Z.; Jia, M.; Dou, X. Observations and analysis of the mid-latitude atmospheric electric field during geomagnetic activity. *J. Geophys. Res. Space Phys.* **2022**, *127*, e2022JA030785. [CrossRef]
43. Scolini, C.; Chané, E.; Temmer, M.; Kilpua, E.K.J.; Dissauer, K.; Veronig, A.M.; Palmerio, E.; Pomoell, J.; Dumbović, M.; Guo, J.; et al. CME–CME Interactions as sources of CME geoeffectiveness: The Formation of the complex ejecta and intense geomagnetic storm in 2017 early September. *Astrophys. J. Suppl. Ser.* **2020**, *247*, 21. [CrossRef]